FRET-based mapping of calmodulin bound to the RyR1 Ca^{2+} release channel

Razvan L. Cornea, Florentin Nitu, Simon Gruber, Katherine Kohler, Michael Satzer, David D. Thomas, and Bradley R. Fruen[1]

Department of Biochemistry, Molecular Biology, and Biophysics, University of Minnesota, 321 Church Street Southeast, Minneapolis, MN 55455

Calmodulin (CaM) functions as a regulatory subunit of ryanodine receptor (RyR) channels, modulating channel activity in response to changing [Ca^{2+}]$_i$. To investigate the structural basis of CaM regulation of the RyR1 isoform, we used site-directed labeling of channel regulatory subunits and fluorescence resonance energy transfer (FRET). Donor fluorophore was targeted to the RyR1 cytoplasmic assembly by preincubating sarcoplasmic reticulum membranes with a fluorescent FK506-binding protein (FKBP), and FRET was determined following incubations in the presence of fluorescent CaMs in which acceptor fluorophore was attached within the N lobe, central linker, or C lobe. Results demonstrated strong FRET to acceptors attached within CaM's N lobe, whereas substantially weaker FRET was observed when acceptor was attached within CaM's central linker or C lobe. Surprisingly, Ca^{2+} evoked little change in FRET to any of the 3 CaM domains. Donor–acceptor distances derived from our FRET measurements provide insights into CaM's location and orientation within the RyR1 3D architecture and the conformational switching that underlies CaM regulation of the channel. These results establish a powerful new approach to resolving the structure and function of RyR channels.

calcium | FKBP | fluorescence | ryanodine receptor | sarcoplasmic reticulum | excitation-contraction coupling

Muscle contraction results from the release of Ca^{2+} from the sarcoplasmic reticulum (SR) through a high-conductance channel known as the ryanodine receptor (RyR). The RyR1 isoform is abundantly expressed in mammalian skeletal muscle and is the largest ion channel identified to date (2.3 MDa). In situ, the homotetrameric RyR1 channel functions in complex with smaller regulatory proteins, which include FK506-binding proteins (FKBPs) and calmodulin (CaM). The interactions between RyR channels and these small regulatory proteins provide important mechanisms for modulating channel structure and function, and altered binding is proposed to underlie life-threatening disorders of SR Ca^{2+} handling (1, 2). However, the structural basis and regulatory significance of these interactions remain unclear, and new approaches for monitoring regulatory protein binding and structural changes within working channels are required.

CaM binds to the RyR1 with a stoichiometry of 4 per channel tetramer (3). In submicromolar Ca^{2+}, apo-CaM binding results in partial activation of RyR1, whereas in micromolar Ca^{2+}, Ca^{2+}CaM binding promotes channel inhibition (4, 5). CaM may therefore function as a resident regulatory subunit of the RyR1, modulating channel gating in response to changing [Ca^{2+}]$_i$. Cryoelectron microscopy (cryo-EM) 3D reconstructions show CaM bound within a cleft that separates the "handle" and "clamp" regions of the RyR1 cytoplasmic assembly (6–8). CaM is thus positioned less than 90 Å from the FKBP subunit, which binds at the opposite edge of the handle region (7, 9). Remarkably, apparent centers of mass of apo-CaM and Ca^{2+}CaM are separated by 33 Å in these cryo-EM structures. This suggests that Ca^{2+}-dependent channel regulation by CaM

may be linked to large-scale structural rearrangements, involving translocation of either CaM itself or of the underlying RyR1 CaM-binding domain (7).

RyR1 proteolysis and mutagenesis have identified a single CaM-binding domain (RyR1$_{3614-3643}$), and synthetic peptides corresponding to this region bind both apo-CaM and Ca^{2+}CaM (3, 10, 11). The atomic structure of Ca^{2+}CaM in complex with the RyR1$_{3614-3643}$ fragment was recently solved by Mackenzie and coworkers (12). Their findings detail the antiparallel binding of Ca^{2+}CaM to the RyR1 target helix first suggested by Hamilton and coworkers (10) and reveal a unique wide spacing of hydrophobic anchors at Trp-3620 and Phe-3636. In binding the RyR1 target, the 2 lobes of Ca^{2+}CaM are therefore positioned apart and do not display the close apposition observed in CaM's complexes with kinase targets (12). Notably, Ca^{2+}-dependent structural rearrangements that underlie CaM regulation are not revealed by the atomic structure of MacKenzie and coworkers (12), and likely involve additional interactions at noncontiguous sites within the full-length RyR1 (12–15). Thus, the relationship between biochemical evidence suggesting a shared binding site for apo-CaM and Ca^{2+}CaM and the large-scale translocations of mass suggested by cryo-EM remains unclear.

To further investigate Ca^{2+}-dependent rearrangements of CaM bound to the RyR1, we have used fluorescence resonance energy transfer (FRET) to monitor distance relationships and structural changes within the intact macromolecular channel. Small FRET acceptors were covalently attached to single-cysteine residues introduced into CaM's N lobe, central linker, or C lobe. The targeting of FRET donors to the RyR1 was accomplished through fluorescent labeling of a single-cysteine FKBP. A key advantage of the FRET-based approach is that existing static structural models may be refined in experiments that examine working channels, in native SR membranes.

Results

Characterization of Labeled Proteins. The 12-kDa FKBPs (FKBPs 12 and 12.6) bind to the RyR1 channel with high affinity and specificity at a defined location on channel's cytoplasmic assembly, and thereby afford a useful means of targeting fluorescent probes within the macromolecular RyR1. The 2 FKBP isoforms similarly suppress the activation of RyR1 channels by Ca^{2+} (16). Of the 2 FKBP isoforms, FKBP12.6 binds RyR1 with 4-fold higher affinity, and it effectively competes with and replaces the native FKBP12 isoform (17). We synthesized a fluorescent FKBP (F-FKBP) FRET donor by site-directed labeling of a
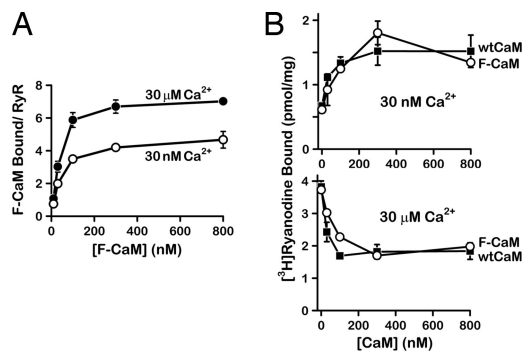
Fig. 1. Binding and regulation of RyR1 channels by an F-CaM in which an acceptor fluorophore is attached within the N lobe. F-CaM binding to SR membranes (*A*) is expressed as ratios of F-CaM bound per ryanodine-binding site. The F-CaM dependence of [³H]ryanodine binding to SR membranes is shown in *B*. Data are means ± SEM from 3–4 experiments.

single-cysteine FKBP12.6 with Alexa Fluor dye (*Materials and Methods*). SR membrane-binding studies demonstrated that the F-FKBP retained high-affinity binding to RyR1 channels and did not dissociate from the channel following washout of unbound F-FKBP (Fig. S1).

A fluorescent CaM (F-CaM) acceptor was synthesized by attaching an acceptor fluorophore at position 34 within CaM's N lobe. Binding of the F-CaM to SR membranes was determined in buffer containing either 30 nM or 30 μM Ca^{2+} (Fig. 1*A*). In 30 nM Ca^{2+}, the F-CaM bound approximately 4 sites per RyR1 tetramer, consistent with RyR1 being the major apo-CaM-binding protein in our SR membrane preparations (15). In 30 μM Ca^{2+}, F-CaM binding was increased by ≈50%, indicating the presence of additional, non-RyR1 binding sites for Ca^{2+}CaM. To directly monitor F-CaM acceptor interactions with RyR1 itself, [³H]ryanodine-binding measurements were also performed (Fig. 1*B*). In 30 nM Ca^{2+}, the F-CaM activated [³H]ryanodine binding to the RyR1 with a concentration dependence similar to unlabeled wild-type CaM. Conversely, in 30 μM Ca^{2+}, both the F-CaM and wild-type CaM inhibited [³H]ryanodine binding. The Ca^{2+} dependence of [³H]ryanodine binding in the absence and in the presence of F-CaM is shown in Fig. S2. These data further demonstrate that the F-CaM and wild-type CaM similarly modulated RyR1 activity over a broad range of [Ca^{2+}], switching from channel activator to channel inhibitor in the presence of ≈1 μM Ca^{2+}. Our ligand-binding studies therefore indicate that the acceptor-labeled CaM retained functional interactions with RyR1 channels that are characteristic of unlabeled apo-CaM and Ca^{2+}CaM.

FRET to CaM's N Lobe. The predicted region of CaM binding on the RyR1 is less than 90 Å from the FKBP site on the same lateral face of the channel (6), and is thus within range of FRET sensitivity. We examined FRET between the F-FKBP donor and the F-CaM acceptor in buffers equivalent to those used in measurements of RyR1 binding and regulation by the F-CaM. Fig. 2*A* shows spectra from a representative experiment in the presence of 30 nM Ca^{2+}. In the absence of F-CaM acceptor, F-FKBP donor excitation resulted in a strong fluorescence signal peaking at 520 nm. In the presence of F-CaM acceptor (100, 300, or 800 nM), a progressive decrease in donor fluorescence was observed, indicating FRET. FRET was abolished in samples in which the F-CaM acceptor was added together with excess unlabeled CaM (Fig. 2*A*, dashed line), indicating that energy transfer was strictly dependent on acceptor binding at high-affinity CaM sites.

Fig. 2*B* shows averaged data from experiments measuring FRET to CaM's N lobe in either 30 nM or 30 μM Ca^{2+}. Energy
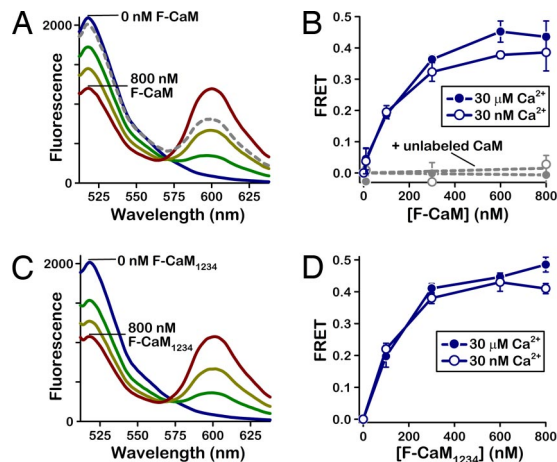

Fig. 2. FRET between a donor-labeled FKBP and acceptor attached within CaM's N lobe. (*A*) Representative spectra in 30 nM Ca^{2+}. Samples contained 0 (blue), 100 nM (green), 300 nM (yellow), or 800 nM (red) F-CaM acceptor. The peak at 520 nm reflects F-FKBP fluorescence (excitation at 490 nm). Peak at 600 nm is F-CaM acceptor. Dashed gray line indicates fluorescence of a sample containing 800 nM F-CaM plus 16 μM unlabeled CaM. (*B*) FRET is plotted as a function of F-CaM acceptor concentration (means ± SEM from 3 experiments). (*C* and *D*) FRET between the F-FKBP donor and a Ca^{2+}-insensitive F-CaM (F-CaM$_{1234}$). Representative spectra were obtained in 30 nM Ca^{2+} and either 0, 100, 300, or 800 nM F-CaM$_{1234}$. Average data are from 3–4 experiments using the F-CaM$_{1234}$.

transfer increased with increasing concentrations of F-CaM acceptor and approached saturation at acceptor concentrations greater than 300 nM (half-maximal FRET in the presence of ≈100 nM F-CaM). The F-CaM dependence of FRET was therefore similar to the F-CaM dependence of [³H]ryanodine binding (Fig. 1 *B* and *C*). Notably, FRET did not significantly differ in samples containing nanomolar and micromolar Ca^{2+} (FRET at 800 nM F-CaM = 0.39 ± 0.06 versus 0.44 ± 0.05 in 30 nM or 30 μM Ca^{2+}, respectively; P = 0.65, paired t test). A further increase in Ca^{2+} (to 300 μM) similarly evoked no significant change in FRET. We conclude that Ca^{2+} has no significant effect on the distance between the donor attached to FKBP and the acceptor attached to CaM's N lobe.

The effect of Ca^{2+} on the proximity of RyR1-bound FKBP and CaM may be determined not only by Ca^{2+} binding to CaM itself, but also by more global structural changes resulting from Ca^{2+} binding to and activation of the underlying RyR1 channel. To resolve Ca^{2+}-dependent structural changes that may occur independently of Ca^{2+} binding to CaM, we also synthesized a fluorescent Ca^{2+}-insensitive CaM in which single E-to-A substitutions were introduced into each of CaM's 4 EF hands (F-CaM$_{1234}$). Previously, we showed that the unlabeled CaM$_{1234}$ mutant activates the RyR1 both in nanomolar and in micromolar Ca^{2+}, effectively functioning as apo-CaM, regardless of [Ca^{2+}] (5, 18). Measurements of F-CaM$_{1234}$ binding to SR membranes indicated that the acceptor bound to approximately 4 sites per RyR1, both in 30 nM and in 30 μM Ca^{2+} (Fig. S3). FRET measurements (Fig. 2 *C* and *D*) demonstrated that energy transfer to the F-CaM$_{1234}$ acceptor was similar to that observed when using the Ca^{2+}-sensitive F-CaM (above), both in terms of the acceptor concentration dependence of FRET and the maximal FRET observed at high acceptor concentrations. Thus, FRET between the F-FKBP donor and the acceptor attached within CaM's N lobe was independent of Ca^{2+} binding to CaM.

Time-Resolved FRET Experiments. Time-resolved measurements of donor fluorescence lifetimes on the nanosecond timescale provide a robust index of FRET that is complementary to steady-
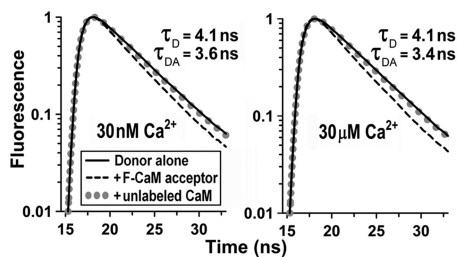
Fig. 3. Time-resolved donor fluorescence decays in the absence and presence of an acceptor attached within CaM's N lobe. Samples contained donor alone (F-FKBP, excitation 355 nm), donor plus acceptor (F-CaM, 800 nM), or donor plus acceptor plus excess unlabeled CaM (16 μM), as indicated in the key. Donor lifetimes in the absence (τ_D) and in the presence (τ_{DA}) of acceptor are based on fits to a 3-exponential decay. Data are from a representative experiment repeated 3 times.

state measurements. To further investigate the effect of Ca^{2+} on FRET to CaM's N lobe, we measured fluorescence lifetimes of an F-FKBP donor in the absence and in the presence of an F-CaM acceptor. To better match the excitation wavelength of our time-resolved instrument, these experiments used a different donor–acceptor dye pair than that used in our steady-state FRET measurements (*Materials and Methods*); however, sample preparation and experimental conditions were the same as in steady-state experiments. In Fig. 3, we show data from a representative time-resolved experiment. In the absence of F-CaM acceptor, the mean lifetime of the F-FKBP donor (τ_D) was the same in 30 nM or 30 μM Ca^{2+} (Fig. 3, solid lines). Addition of F-CaM (Fig. 3, dashed lines) evoked a decrease in donor lifetime (τ_{DA}), which was fully reversed upon further addition of excess unlabeled CaM (Fig. 3, dotted lines). FRET, calculated as the fractional decrease in donor lifetime in the presence of acceptor (Eq. 1), did not significantly differ in 30 nM and 30 μM Ca^{2+} (FRET = 0.13 $\pm$ 0.01 versus 0.16 $\pm$ 0.01, respectively; P = 0.13, n = 3 paired experiments). These time-resolved measurements thus validate our steady-state measurements, indicating that FRET between FKBP and CaM's N lobe was similar in the absence and in the presence of micromolar Ca^{2+}.

FRET to CaM's Central Linker and C Lobe. In subsequent experiments, we investigated how steady-state FRET between RyR1-bound FKBP and CaM may vary as a function of the position of the acceptor fluorophore within CaM's primary structure. These experiments addressed the possibility that Ca^{2+}-dependent structural rearrangements of CaM on RyR1 may be limited to a particular lobe of CaM. For these experiments, we synthesized F-CaM acceptors in which the acceptor fluorophore was shifted from CaM's N lobe to either the central linker (position 75) or the C lobe (position 110). [^{3}H]ryanodine-binding measurements demonstrated that F-CaMs labeled within either the central linker or C lobe retained the capability to bind and regulate RyR1 (Fig. S2). FRET measurements (Fig. 4) indicated that energy transfer to acceptor attached within the central linker was only half that observed when the acceptor was attached to CaM's N lobe. When the acceptor was attached to CaM's C lobe, the reduction in FRET was more pronounced ($\approx$25% of FRET to CaM's N lobe). Results in Fig. 4 thus suggest that CaM's N lobe is nearest and the C lobe farthest from the F-FKBP donor. Small differences in FRET in the presence of 30 nM versus 30 μM Ca^{2+} were not statistically significant. However, a trend toward slightly increased FRET in micromolar Ca^{2+} was evident for each of the 3 domains of CaM (Fig. 4).
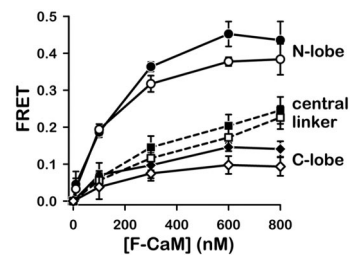
Fig. 4. FRET to an acceptor attached within CaM's central linker or C lobe. Data are means $\pm$ SEM from 4–6 experiments in either 30 nM Ca^{2+} (open symbols) or 30 μM Ca^{2+} (filled symbols). FRET to the N lobe of CaM is replotted from Fig. 2B for comparison.

Does Donor–Acceptor Binding to Non-RyR Targets Contribute to FRET? To address the possibility that the binding of F-FKBPs or F-CaMs at non-RyR1 sites may contribute to our FRET results, we also examined FRET in experiments using purified RyR1 channels. Solubilized SR membrane fractions enriched in RyR1 were identified by [^{3}H]ryanodine binding and characterized by SDS/PAGE (Fig. 5A). The purity of the high-molecular weight RyR1 was estimated at >94% by gel densitometry analysis. Experiments directly compared FRET between FKBP and CaM in samples containing either intact SR membranes (Fig. 5B) or purified RyR1 (Fig. 5C). Strong energy transfer to CaM's N lobe was observed whether samples contained intact SR membranes or purified RyR1 (FRET $\approx$ 0.4). The relative efficiency of FRET to the different domains of CaM was also similar for the different preparations (FRET to N lobe > central linker > C lobe). Finally, both SR membranes and purified RyR1 samples displayed only small increases in FRET when Ca^{2+} was increased from 30 nM to 30 μM (Fig. 5 B and C). Results therefore indicate that the observed FRET between FKBP and CaM was a function of specific binding of donors and acceptors to the RyR1 itself, and that binding at additional, non-RyR1 sites is unlikely to confound the evaluation of our FRET results.

Evaluation of Donor–Acceptor Distances. FRET provides a sensitive measure of donor–acceptor distances because of the inverse sixth-power dependence of energy transfer on distance near the Förster radius (R_0) of a given donor–acceptor pair (Eq. 2). The R_0 of the donor–acceptor pair in our steady-state FRET exper-
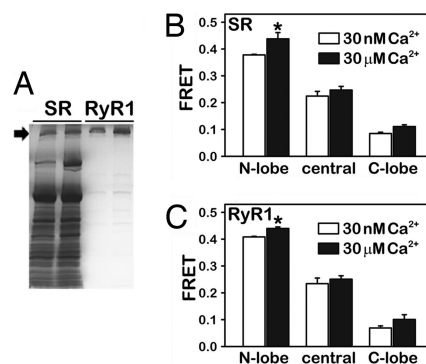
Fig. 5. Comparison of FRET in samples containing intact SR membranes and solubilized, purified RyR1. (*A*) Coomassie-stained gel comparing 2 SR membrane and 2 RyR1 preparations. Arrow points to 565-kDa RyR1 monomer. (*B* and *C*) FRET between F-FKBP donor and acceptor attached within CaM's N lobe, C lobe, or central linker. Experiments shown in *B* and *C* examined the same preparations shown in *A*. Samples contained 800 nM F-CaM acceptor and either 30 nM or 30 μM Ca^{2+}, as indicated. Asterisks indicate significant differences from corresponding values at 30 nM Ca^{2+}. Data are means $\pm$ SE from 4 experiments.
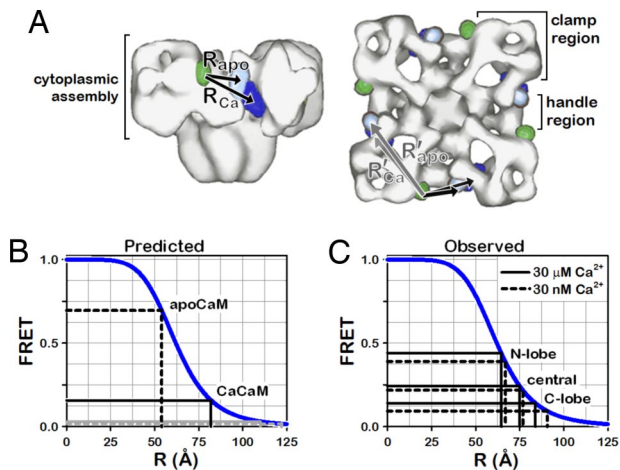
Fig. 6. Evaluation of predicted and observed donor–acceptor distances (*R*). (*A*) RyR1 cryo-EM structural models (6, 7) showing proximities of apo-CaM (light blue) and Ca^{2+}CaM (dark blue) to FKBP (green). Channel is shown in side view (*Left*) and top view (*Right*). (*B*) Predicted FRET between FKBP and the apo-CaM and Ca^{2+}CaM species, based on proximities of FKBP and CaM centers of mass in cryo-EM models and the R_0 of the donor–acceptor pair. (*C*) Observed donor–acceptor distances derived from steady-state FRET measurements.

iments was 62 Å, indicating good sensitivity to molecular distances in the range of 31–93 Å. The predicted distances (*R*) separating RyR1-bound FKBP and CaM in cryo-EM structural models (7) are shown in Fig. 6*A*. These models predict that FKBP and apo-CaM centers of mass on the same lateral face of the channel are separated by 54 ± 5 Å (R_{apo} in Fig. 6*A*). We therefore expect that energy transfer between our F-FKBP donor and F-CaM acceptor would be strong in the presence of submicromolar Ca^{2+} (predicted FRET = 0.7; Fig. 6*B*). By comparison, these simulations predict much weaker energy transfer in the presence of micromolar Ca^{2+} (R_{Ca}; predicted FRET = 0.16) because of the 33-Å shift in the apparent center of mass of Ca^{2+}CaM bound to RyR1 (7). Note that predicted distances to CaM on the adjacent face of the channel are greater ($R'_{apo} = 122 \pm 5$ Å, $R'_{Ca} = 110 \pm 5$ Å; Fig. 6*A*) and are expected to contribute less than 4% to the FRET signal (Fig. 6*B*, gray lines). Similarly, distances to CaM on neighboring channels within multichannel arrays (19) are predicted to exceed 130 Å and to be well beyond the range of FRET sensitivity.

Observed distances derived from steady-state FRET between donor-labeled FKBP and acceptors attached within the 3 domains of CaM are shown in Fig. 6*C*. The data indicate that the acceptor is nearest to the F-FKBP donor when attached to CaM's N lobe ($R = 67 \pm 3$ Å and 65 ± 3 Å in 30 nM and 30 μM Ca^{2+}, respectively). When the acceptor was attached within CaM's C lobe, donor–acceptor separation was increased by ≈20 Å ($R = 91 \pm 9$ Å and 84 ± 5 Å in 30 nM and 30 μM Ca^{2+}, respectively), whereas the proximity of the central linker was intermediate to that of 2 lobes. The observed proximities of each of the 3 CaM domains are well within the limits of CaM–FKBP proximities predicted by RyR1 cryo-EM (Fig. 6*B*). However, our FRET-based distance measurements clustered nearer to the predicted proximity of the Ca^{2+}CaM species. Most notably, all observed donor–acceptor distances derived from FRET were similar in nanomolar and micromolar Ca^{2+}, trending toward a slight decrease in separation in the presence of micromolar Ca^{2+}. This is in clear contrast to predictions based on cryo-EM.

The R_0 of the donor–acceptor pair in our time-resolved FRET experiments was 50 Å, which is significantly less than the 62 Å R_0 of our steady-state donor–acceptor pair. Consequently, these measurements were sensitive to a shorter range of donor–

acceptor distances (25–75 Å). Donor–acceptor distances derived from time-resolved FRET showed excellent agreement with the corresponding distances derived from steady-state measurements of FRET to CaM's N lobe (time-resolved $R = 69 \pm 1$ Å and 66 ± 1 Å in 30 nM and 30 μM Ca^{2+}, respectively). These time-resolved results, obtained by using a different method, a different instrument, and a different dye pair, therefore strengthen our confidence in the distances derived from our steady-state measurements. Because of the shorter R_0 of the donor–acceptor pair in these time-resolved experiments, these data also support the conclusion that FRET was a simple function of the proximity of nearest-neighbor donor–acceptor pairs within the tetrameric RyR1, and that longer-range interactions (>75 Å) did not significantly contribute to the FRET signal.

Discussion

We have used FRET to monitor the binding and orientation of CaM within the intact, macromolecular RyR1 channel in native SR membranes. To test the hypothesis that CaM undergoes large-scale rearrangements upon binding Ca^{2+}, we measured distances between donor fluorophores attached to the FKBP subunit and acceptors attached within discrete structural domains of CaM.

FRET Reflects CaM Binding to RyR1 Channels. Our results support the conclusion that FRET between our donors and acceptors bound to SR membranes is a function of binding to RyR1 itself. Accordingly, we found that the F-CaM dependence of FRET in the absence and presence of micromolar Ca^{2+} (Fig. 2) mirrored the F-CaM dependence of RyR1 activation and inhibition in [^{3}H]ryanodine measurements (Fig. 1*B*). Furthermore, solubilization and purification of RyR1 to remove non-RyR targets did not affect the efficiency of FRET between FKBP and the different domains of CaM (Fig. 5). All FRET-based distance measurements were well within the limits of CaM–FKBP proximities predicted by RyR1 cryo-EM (Fig. 6). Finally, we found that the proximity of F-FKBP donors and acceptors attached within CaM's N and C lobes differed by ≈20 Å (Fig. 6*C*). These marked positional differences are consistent with the uniquely wide spacing of the N and C lobes that is evident in the atomic structure of the CaM in complex with the RyR1$_{3614–3643}$ target (22-Å separation of CaM residues 34 and 110) (12). Thus, although non-RyR targets comprise a significant fraction of the Ca^{2+}CaM-binding sites in our membrane preparations, the use of an F-FKBP donor with high affinity and high selectivity for RyR channels has allowed us to effectively tease out CaM interactions with the RyR1.

Ca^{2+} Evokes Little or No Change in FRET. Ca^{2+} binding to CaM results in CaM's conversion from RyR1 activator to RyR1 inhibitor (3, 4), and CaM inhibition is abolished by EF-hand mutations that impair Ca^{2+} binding (5). It is therefore clear that Ca^{2+} binding elicits functionally important structural changes within the CaM–RyR1 complex. The molecular details of these structural changes are not yet clear.

Cryo-EM mapping of RyR1-bound CaM in the absence and in the presence of Ca^{2+} has indicated that CaM's conversion from channel activator to channel inhibitor may be linked to a large-scale translocation of CaM (7). However, when we compared FRET under buffer conditions in which CaM either activates or inhibits RyR1, we observed little change in FRET (Figs. 2–5). Moreover, we found that FRET between FKBP and CaM was unaffected by EF-hand mutations that impair Ca^{2+} binding to CaM (Fig. 2 *C* and *D*). These results indicate that distance relationships between FKBP and CaM are largely unaffected by Ca^{2+} binding to either CaM or the underlying RyR1. Our results do not entirely rule out the possibility that

Fig. 7. Suggested placement of CaM within the RyR1 3D architecture. (*A*) (*Left*) The RyR1 cryo-EM structure (EMBL 1275) is shown in side view. (Scale bar: 100 Å.) The dashed red circle indicates the FKBP-binding site (6), and the red dot approximates the predicted position of donor fluorophore attachment based on the model of Samsó et al. (9). The dashed blue oval approximates the site of Ca^{2+}CaM binding within the cleft separating cytoplasmic domains 3 and 8 (7). (*Right*) Atomic structure of Ca^{2+}CaM in complex with $RyR1_{3614-3640}$ (PDB 2BCX). Positions of acceptor attachment within CaM's N lobe and C lobe are highlighted in red (labeling site within the central linker is obscured). (*B*) Proposed placement of CaM. A space-filling representation of CaM–$RyR1_{3614-3640}$ is positioned within the channel cleft and oriented such that the N lobe is nearest and C lobe farthest from FKBP, as indicated by FRET. The figure was prepared by using University of California, San Francisco Chimera software.

large-scale translocations of CaM occur along an arc of constant radius from the FKBP donor. Similarly, the possibility that the FKBP and CaM subunits move in parallel with changing $[Ca^{2+}]$ should be considered. However, cryo-EM studies to date have provided no indication of large-scale translocations involving the FKBP subunit, and our own studies show no effect of Ca^{2+} on the affinity or stoichiometry of FKBP binding to RyR1 ([Fig. S1](#)). Therefore, we conclude that Ca^{2+} switching involves comparatively subtle structural rearrangements at the CaM–RyR1 interface. These rearrangements may include changes in CaM's interactions with the core $RyR1_{3614-3643}$ target sequence, changes in CaM's interactions with noncontiguous sites within the channel primary structure, or rotation of CaM about its major axis (10, 13, 14).

Suggested Placement of CaM Within the RyR1 3D Architecture. Our results suggest new insights into the location and orientation of CaM on the RyR1 when considered in context with existing structural models. In Fig. 7*A Left*, a recent cryo-EM model of the 2.3-MDa RyR1 (20) is shown, with the positions of FKBP and CaM binding indicated by dashed ovals. Fig. 7*A Right* shows the atomic model of Ca^{2+}CaM in complex with the $RyR1_{3614-3640}$ target (12). In Fig. 7*B*, we have positioned a space-filling representation of the CaM–$RyR1_{3614-3640}$ complex within the cleft separating the handle and clamp regions of the RyR1 cytoplasmic assembly, as indicated by cryo-EM mapping of Ca^{2+}CaM (6, 7). CaM's position and orientation were manipulated until distance relationships between the site of FKBP binding and sites of fluorescent labeling within CaM's N and C lobes were in agreement with distances derived from our FRET measurements.

The placement of CaM in Fig. 7*B* is consistent with the position of Ca^{2+}CaM in RyR1 cryo-EM models (6). In partic-

ular, these models show Ca^{2+}CaM as an elongated mass, with one end adjacent to the handle region (domain 3) and the other end extending beneath the clamp region. In our model, the domain of CaM nearest to FKBP and adjacent to the handle region is identified as the N lobe, whereas the C lobe is placed beneath the clamp region. The model thus positions CaM's N and C lobe Ca^{2+}-binding sites within distinct microdomains of the channel. This is of interest in light of the distinct roles played by CaM's N and C lobes in regulating other ion channels (21, 22). The location of the $RyR1_{3614-3643}$ target helix within the domain structure of the channel is not defined in existing structural models. In our model, the target helix is placed near the outer edge of domain 3 (Fig. 7*A*). Alternatively, the target helix may also lie along the edge of domain 8 without significantly changing distance relationships between CaM and FKBP.

In conclusion, we describe a new approach to RyR structure/function, in which small fluorescent reporters are attached to discrete domains of FKBP and CaM, and FRET is used to monitor regulatory protein binding, structural changes, and distance relationships within working channels. Our results provide new insights into the structural basis of channel regulation by CaM, and they help bridge the different levels of understanding provided by available cryo-EM models of intact, solubilized channels and atomic models of channel fragments and subunits. We expect that this approach may be readily extended to investigations of SR Ca^{2+} release in other experimental systems, including intact, permeabilized myocytes.

Materials and Methods

Materials. Skeletal muscle SR membrane vesicles were isolated from pig longissimus dorsi muscle by differential ultracentrifugation of homogenized muscle (5, 18). Samples enriched in RyR1 were obtained by sucrose gradient fractionation of CHAPS-solubilized SR (23). Cysteine-reactive fluorescent dyes were purchased from Invitrogen/Molecular Probes. [³H]ryanodine was from Perkin–Elmer.

Expression, Purification, and Fluorescent Labeling of Single-Cysteine Mutants of FKBP and CaM. A single-cysteine FKBP (T14C, C22A, C76I FKBP12.6) was derived from the human FKBP12.6 cDNA by site-directed mutagenesis (QuikChange kit; Stratagene) and expressed in *Escherichia coli* BL21(DE3)pLysS, and the FKBP was purified as described previously (24, 25). Single-cysteine CaMs with substitutions within either the N lobe (T34C), central linker (K75C), or C lobe (T110C) were expressed and purified as described previously (5, 15). A single-cysteine Ca^{2+}-insensitive CaM was synthesized by introducing the T34C substitution into a CaM_{1234} mutant (E–to-A substitutions at positions 31, 67, 104, and 140) (5).

The FKBP mutant was labeled at its single cysteine by using maleimide derivatives of either Alexa Fluor 488 or Alexa Fluor 350. Unreacted dye was removed by chromatography on DEAE Sephacel (Sigma–Aldrich), and the sample was dialyzed and concentrated by using an Amicon device (Millipore) into 20 mM MOPS and 30 mM NaCl, pH 7.0, at a protein concentration of 60–100 μM.

Single-cysteine CaMs were labeled with either Alexa Fluor 568 or Alexa Fluor 488 and applied to phenyl-Sepharose columns to remove unreacted dye (15). F-CaMs were dialyzed and concentrated as described above for F-FKBPs. Essentially, stoichiometric labeling of F-CaMs was demonstrated by the absorbance of the bound dye and SDS/PAGE densitometry of F-CaM protein, and it was confirmed by MALDI-TOF mass spectrometry (≥95% labeling in each case).

Ligand-Binding Studies. The binding of F-CaMs to SR membranes (0.4 mg/mL) was measured following 2.5-h incubations in buffer containing 150 mM KCl, 20 mM K-piperazine-N-N′-bis(2-ethanesulfonic acid (K-Pipes; pH 7.0), 5 mM reduced glutathione, 0.1 mg/mL BSA, 1 μg/mL aprotinin/leupeptin, 1 mM EGTA, and sufficient $CaCl_2$ to achieve the desired Ca^{2+} concentration (26). Nonspecific binding was measured in the presence of 20 μM unlabeled CaM. Bound F-CaM and free F-CaM were separated by centrifugation at 100,000 × *g*. Pellets were dissolved in 5% SDS, 50 mM NaCl, 20 mM Na-Pipes (pH 7.0), and 1 mM EGTA, and bound F-CaM was determined from the fluorescence intensity at 595 nm (560-nm excitation, 570-nm emission long-pass filter). The binding of [³H]ryanodine (20 nM) to SR membranes was determined following 16-h incubations in the same binding buffer containing 0.2 mg/mL SR protein (5).

FRET Measurements. Steady-state FRET experiments used Alexa Fluor 488-FKBP and Alexa Fluor 568-CaM as a donor–acceptor pair ($R_0 = 62$ Å) (27). SR membranes (0.4 mg/mL) were preincubated with the F-FKBP (50 nM) for 90 min in the KCl/Pipes-binding buffer. Membranes were centrifuged at $100{,}000 \times g$ to remove unbound F-FKBP donor, and the pellet was resuspended to a final concentration of 3 mg/mL. FRET was measured following 2.5-h incubations at 25 °C in the same buffer containing 0–800 nM F-CaM acceptor. Steady-state fluorescence emission spectra were acquired in 384-well, optical-bottom, black plates by using a Gemini EM microplate fluorometer (Molecular Devices) with excitation at 490 nm and a 495-nm emission long-pass filter.

Time-resolved FRET experiments used Alexa Fluor 350-FKBP and Alexa Fluor 488-CaM as a donor–acceptor pair ($R_0 = 50$ Å). Fluorescence was excited with a nanosecond laser pulse and detected with subnanosecond resolution by using a custom fluorometer built by Igor Negrashov in collaboration with Fluorescence Innovations Inc. Excitation at 355 nm was provided by a 9-kHz, frequency-tripled, Q-switched microchip YAG laser (NanoUV-355; JDS Uniphase), and emission was directly converted to digital form via an 8-bit, 0.125 ns per channel DS252 digitizer (Acqiris, Geneva, Switzerland). Full-fluorescence waveforms were acquired after each laser pulse with 0.2 ns per data point resolution. The instrument–response function was acquired by detecting light scattering with the same instrument settings as for the samples.

Analysis of FRET Data. FRET efficiency was calculated from the decrease of donor steady-state fluorescence (F_D) due to the presence of acceptor (F_{DA}), or from the average fluorescence lifetimes τ_D and τ_{DA}, according to

$$FRET = \left(1 - \frac{F_{DA}}{F_D}\right) = \left(1 - \frac{\tau_{DA}}{\tau_D}\right). \qquad [1]$$

Donor–acceptor distances, R, were calculated from

$$R = R_0(FRET^{-1} - 1)^{1/6}, \qquad [2]$$

where R_0 is defined as the distance at which FRET = 0.5. Lifetimes were determined from time-resolved fluorescence, which was analyzed by using a multiexponential function

$$F(t) = F_0 \sum_{i=1}^{n} x_i e^{-t/\tau_i}, \qquad [3]$$

where τ_i and x_i are the excited-state lifetimes and mole fractions, respectively. This function was convoluted with the instrument–response function and fit to the experimental data. F_0, τ_i, and x_i were varied to minimize χ^2, increasing n until there was no significant decrease in χ^2 with further increase in n. This typically resulted for $n = 3$. Distance measurements assumed random orientation of fluorophores. This assumption is supported by the agreement of distance measurements with different donor–acceptor pairs.

1. Bers DM (2004) Macromolecular complexes regulating cardiac ryanodine receptor function. *J Mol Cell Cardiol* 37:417–429.
2. Zalk R, Lehnart SE, Marks AR (2007) Modulation of the ryanodine receptor and intracellular calcium. *Annu Rev Biochem* 76:367–385.
3. Moore CP, et al. (1999) Apocalmodulin and Ca²⁺ calmodulin bind to the same region on the skeletal muscle Ca²⁺ release channel. *Biochemistry* 38:8532–8537.
4. Tripathy A, Xu L, Mann G, Meissner G (1995) Calmodulin activation and inhibition of skeletal muscle Ca²⁺ release channel (ryanodine receptor). *Biophys J* 69:106–119.
5. Fruen BR, et al. (2003) Regulation of the RYR1 and RYR2 Ca²⁺ release channel isoforms by Ca²⁺-insensitive mutants of calmodulin. *Biochemistry* 42:2740–2747.
6. Wagenknecht T, et al. (1997) Locations of calmodulin and FK506-binding protein on the three-dimensional architecture of the skeletal muscle ryanodine receptor. *J Biol Chem* 272:32463–32471.
7. Samsó M, Wagenknecht T (2002) Apocalmodulin and Ca²⁺-calmodulin bind to neighboring locations on the ryanodine receptor. *J Biol Chem* 277:1349–1353.
8. Samsó M, Wagenknecht T, Allen PD (2005) Internal structure and visualization of transmembrane domains of the RyR1 calcium release channel by cryo-EM. *Nat Struct Mol Biol* 12:539–544.
9. Samsó M, Shen X, Allen PD (2006) Structural characterization of the RyR1-FKBP12 Interaction. *J Mol Biol* 356:917–927.
10. Rodney GG, et al. (2001) Calcium binding to calmodulin leads to an N-terminal shift in its binding site on the ryanodine receptor. *J Biol Chem* 276:2069–2074.
11. Yamaguchi N, Xin C, Meissner G (2001) Identification of apocalmodulin and Ca²⁺-calmodulin regulatory domain in skeletal muscle Ca²⁺ release channel, ryanodine receptor. *J Biol Chem* 276:22579–22585.
12. Maximciuc AA, Putkey JA, Shamoo Y, Mackenzie KR (2006) Complex of calmodulin with a ryanodine receptor target reveals a novel, flexible binding mode. *Structure* 14:1547–1556.
13. Zhang H, Zhang JZ, Danila CI, Hamilton SL (2003) A noncontiguous, intersubunit binding site for calmodulin on the skeletal muscle Ca²⁺ release channel. *J Biol Chem* 278:8348–8355.
14. Yamaguchi N, Xu L, Evans KE, Pasek DA, Meissner G (2004) Different regions in skeletal and cardiac muscle ryanodine receptors are involved in transducing the functional effects of calmodulin. *J Biol Chem* 279:36433–36439.
15. Fruen BR, et al. (2005) Direct detection of calmodulin tuning by ryanodine receptor channel targets using a Ca²⁺-sensitive acrylodan-labeled calmodulin. *Biochemistry* 44:278–284.
16. Barg S, Copello JA, Fleischer S (1997) Different interactions of cardiac and skeletal muscle ryanodine receptors with FK-506 binding protein isoforms. *Am J Physiol* 272:C1726–C1733.
17. Xin HB, Rogers K, Qi Y, Kanematsu T, Fleischer S (1999) Three amino acid residues determine selective binding of FK506-binding protein 12.6 to the cardiac ryanodine receptor. *J Biol Chem* 274:15315–15319.
18. Fruen BR, Bardy JM, Byrem TM, Strasburg GM, Louis CF (2000) Differential Ca²⁺ sensitivity of skeletal and cardiac muscle ryanodine receptors in the presence of calmodulin. *Am J Physiol* 279:C724–C733.
19. Yin CC, D'Cruz LG, Lai FA (2008) Ryanodine receptor arrays: Not just a pretty pattern? *Trends Cell Biol* 18:149–156.
20. Serysheva II, et al. (2008) Subnanometer-resolution electron cryomicroscopy-based domain models for the cytoplasmic region of skeletal muscle RyR channel. *Proc Natl Acad Sci USA* 105:9610–9615.
21. Saimi Y, Kung C (1994) Ion channel regulation by calmodulin binding. *FEBS Lett* 350:155–158.
22. Tadross MR, Dick IE, Yue DT (2008) Mechanism of local and global Ca²⁺ sensing by calmodulin in complex with a Ca²⁺ channel. *Cell* 133:1228–1240.
23. Lai FA, Erickson HP, Rousseau E, Liu QY, Meissner G (1988) Purification and reconstitution of the calcium release channel from skeletal muscle. *Nature* 331:315–319.
24. Holzman TF, et al. (1991) Preliminary characterization of a cloned neutral isoelectric form of the human peptidyl prolyl isomerase cyclophilin. *J Biol Chem* 266:2474–2479.
25. Park ST, Aldape RA, Futer O, DeCenzo MT, Livingston DJ (1992) PPIase catalysis by human FK506-binding protein proceeds through a conformational twist mechanism. *J Biol Chem* 267:3316–3324.
26. Brooks SPJ, Storey KB (1992) Bound and determined: A computer program for making buffers of defined ion concentrations. *Anal Biochem* 201:119–126.
27. Haugland RP, Spence MTZ, Johnson ID, Basey A (2005) *The Handbook: A Guide to Fluorescent Probes and Labeling Technologies* (Molecular Probes, Eugene, OR).

BIOPHYSICS AND
COMPUTATIONAL BIOLOGY